SPHERICALLY EXPANDING FLAME SIMULATIONS IN CANTERA USING A LAGRANGIAN FORMULATION

Maxwell, B.M.[1], Mével, R.[2], and Melguizo-Gavilanes, J.[3]

[1]Department of Mechanical and Aerospace Engineering, Case Western Reserve University,
[2]Center for Combustion Energy, School of Vehicle and Mobility, Tsinghua University,
[3]Institut Pprime, UPR 3346 CNRS, ISAE-ENSMA,
brian.maxwell@case.edu

Abstract

A Lagrangian-based one-dimensional approach has been developed using Cantera to study the dynamics of spherically expanding flames. The detailed reaction model USC-Mech II has been employed to examine flame propagating in hydrogen-air mixtures. In the first part, our approach has been validated against laminar flame speed and Markstein number data from the literature. It was shown that the laminar flame speed was predicted within 5% on average but that discrepancies were observed for the Markstein number, especially for rich mixtures. In the second part, a detailed analysis of the thermo-chemical dynamics along the path of Lagrangian particles propagating in stretched flames was performed. For mixtures with negative Markstein lengths, it was found that, at high stretch rates, the mixture entering the reaction-dominated period is less lean with respect to the initial mixture than at low stretch rate. This induces a faster rate of chemical heat release and of active radical production which results in a higher flame propagation speed. Opposite effects were observed for mixtures with positive Markstein lengths, for which slower flame propagation was observed at high stretch rates compared to low stretch rates.

1. INTRODUCTION

Nowadays, hydrogen is mainly used as a chemical in specialized industries such as ammonia and methanol synthesis and hydrogenation of fats and oils [1]. In the future, hydrogen may become a widely used energy carrier both for economical and environmental reasons [2]. This perspective, along with other advantages of hydrogen in terms of efficiency increase and emission reduction [3–7], has motivated extensive work on hydrogen-enriched fuel blends for gas turbine and combustion engines [3–6, 8–10]. However, since the combustion of these lean mixtures is subject to thermo-diffusive instabilities, significant technical and engineering challenges arise in order to avoid unstable combustion, flash-back, blow-off, and noise [11]. The spread of hydrogen use to non-specialists also involves serious safety concerns. The study of hydrogen combustion properties is also important for the risk assessment of nuclear activities. Past and recent accidental events, for example in the United States at Three Mile Island [2] and in Japan at Fukushima nuclear complex, have demonstrated the continuing relevance of studying hydrogen-air combustion.

Flames propagating in mixtures with negative Markstein lengths (or numbers), such as lean hydrogen-air mixtures, are well known to develop cellular instability at an early stage of the propagation [2, 12, 13]. The cellularity of flames is a result of the competition between a number of phenomena including hydrodynamic instability, preferential diffusion and flame stretch [2]. As a cellular flame front develops,

the flame area increases and the flame accelerates [14, 15]. This early phase of acceleration might play an important role in the flame acceleration process and possible subsequent transition to detonation (DDT) [16]. In this regard, flame propagation in lean hydrogen–air, with negative Markstein lengths, are very likely to develop unstable flame wrinkling, which would result in increased burning rates and even influence flame acceleration to the point of choking. On the other hand, the stabilizing effect of preferential-diffusion and stretch for rich mixtures also influences the flame acceleration process by delaying the development of a cellular flame structure. As a consequence, a detailed characterization of the response of the flame to stretch is of primary importance for risk assessments. A large number of studies have examined numerically the flame structure and dynamics for hydrogen-air mixtures. Among other studies, Aung et al. [17] investigated the effect of stretch on the laminar flame structure using one-dimensional (1-D) numerical simulation of spherical flame. They noted an increase/decrease of temperature and radicals concentration for mixtures with negative/positive Markstein length as compared to unstretched freely propagating flames. Kwon and Faeth [18] performed a similar study for hydrogen-oxygen mixtures diluted with helium and argon. Sun et al. [19] employed outwardly and inwardly propagating 1-D flames to extract the global parameters of hydrogen-air flames. More recently, Varea et al. [20] employed the A-SURF code to simulate outwardly propagating spherical flame in lean hydrogen-air mixtures and compared their results with experimental data. Despite the great insights provided by numerical simulation of unsteady, one-dimensional (1-D) spherically expanding flames, it is noted that such an approach has not been fully generalized in the combustion community and that, to the best of our knowledge, such a code is still not freely available.

The purpose of the present study was to develop and validate a code to simulate unsteady, one-dimensional spherically expanding flames with plans to make it widely available to the combustion community as open source software. Here, we chose to implement a Lagrangian-based 1-D simulation framework using Cantera and Sundials CVODE libraries. While such unsteady Lagrangian flame codes have been popular in the past (i.e. Run-1DL [21]), none are open source or freely available. For validation, we intended to reproduce experimental macroscopic flame properties such as the laminar flame speed and the Markstein number. Then, we employ our code to examine the flame dynamics of lean hydrogen-air mixtures.

2. NUMERICAL SIMULATIONS

2.1. Numerical method

We considered the one-dimensional unsteady evolution of a laminar flame in spherical coordinates. Here, the flame evolution was governed by diffusion-reaction equations for a chemically reactive fluid augmented by the evolution of each chemically reactive species. To simplify the governing equations, the low-Mach number approximation [22] was applied. Also, unsteady temporal pressure changes were neglected. As a result, the conservation evolution of each chemical species and sensible enthalpy was decoupled from the conservation of momentum equation. Finally, mass-weighted Lagrangian coordinates were considered, as previously adopted to investigate the spontaneous ignition of high pressure hydrogen jets into air [23], turbulent combustion subgrid closure via CLEM-LES [24], and also asymptotic analysis of stretched flames [25]. This strategy was originally used in the former Run-1DL code [21], which was often used to simulate 1D flames in many past investigations, i.e. [17, 26–31]. This strategy effectively eliminated the requirement to solve the continuity equation and the velocity field. This also eliminated $(1/r)$ terms normally present in radial coordinate formulations, and therefore eliminated the singularity problem as $r \rightarrow 0$ where r is the radius. The resulting system of equations which was solved

was

$$\underbrace{\rho\frac{\partial Y_i}{\partial t}}_{\Delta \text{ mass (specie i)}} = \underbrace{\dot{\omega}_i}_{\text{production rate}} - \underbrace{\rho\frac{\partial(\rho r^2 u_{d,i} Y_i)}{\partial m}}_{\text{diffusion}} \tag{1}$$

$$\underbrace{\rho c_p \frac{\partial T}{\partial t}}_{\Delta \text{ enthalpy}} = \underbrace{\rho\frac{\partial}{\partial m}\left(\rho r^4 k \frac{\partial T}{\partial m}\right) - \sum_{i=1}^{N} \rho^2 r^2 c_{p,i} u_{d,i} Y_i \frac{\partial T}{\partial m}}_{\text{diffusion}} - \underbrace{\sum_{i=1}^{N} h_i \dot{\omega}_i}_{\text{heat release}} \tag{2}$$

In this approach, a transformation from radial to mass-weighted Lagrangian coordinates was applied, i.e. $(r, t) \rightarrow (m, t)$, where the mass-based coordinate, m, was obtained by integrating

$$m(r,t) = \int_{r=0}^{r} \rho r^2(r,t) dr \tag{3}$$

In (1)-(3), h_i is specific enthalpy of the ith species, k is the thermal conductivity for the mixture, m is the mass coordinate (Lagrangian coordinate), p is the pressure, T is the temperature, t is the time, $u_{d,i}$ is the diffusion velocity of the ith species (which includes ordinary, thermal, and correction velocity components, depending on the transport properties adopted), r is the radius, Y_i is the mass fraction of the ith species, ρ is the density, and $\dot{\omega}_i$ is the net rate of production of the ith species.

To solve the equation set (1)-(2), an operator splitting technique [32] was applied. The solution was first obtained for the inert diffusion terms across one time step using the explicit Forward Euler method [33] and upwind differencing. The production and heat release terms were then solved implicitly across the same time step using the Sundials CVODE solver [34]. Currently, we do not employ adaptive mesh-refinement, however the code is parallelized for shared memory systems using OpenMP libraries [35]. Ongoing efforts are being made to the eliminate operator-splitting and to develop a fully implicit and parallelized code in the Sundials CVODE framework. Cantera 2.4 [36] libraries were used to incorporate the USC-Mech II detailed chemical kinetic mechanism, using both mixture-averaged [37, 38] and multi-component [39] transport properties.

For each simulation, up to 5000 computational nodes were used. The resolutions, Δm, were chosen for each simulation such that the flame radius could be recorded in the range 8mm $< r <$ 24mm. Grid convergence tests were also conducted to ensure that the chosen resolutions produced converged flame speed solutions within this range. To initiate a flame simulation, a pocket of burned gas was specified within the first 20 to 40 computational nodes. The temperature and composition of the burned gas was estimated by allowing the gas, in this region, to reach chemical equilibrium at constant enthalpy and pressure prior to simulation. To avoid computational difficulties associated with sharp gradients at startup, a smoothing function [40] across 6 computational nodes was applied at the interface between burned and unburned gas. Finally, zero-gradient conditions were prescribed at both boundaries.

2.2. Reaction model

The well established reaction model of Davis et al. [41], referred to as USC-Mech II, has been selected for the present study. It includes 10 chemical species and 28 reversible reactions. Nitrogen was considered inert and thus, NO_x chemistry was neglected. The transport data provided with this model were employed to calculate the transport properties.

3. RESULTS AND DISCUSSION

3.1. Prediction of macroscopic flame properties

This section focuses on the prediction of macroscopic flame properties, namely the laminar flame speed and the Markstein number. Numerical simulations have been performed over the range of equivalence ratios ϕ=0.3 to 5 at T_1=300 K and p_1=101 kPa. In order to extract the relevant quantities from the 1-D simulations, the linear extrapolation model has been employed. This approach was motivated by the fact that in many studies, the flame properties have been extracted using this method. Briefly, from asymptotic analysis performed in the limit of high activation energy and low stretch rate [42–44], the spatial flame speed (S_b) is given by

$$S_b = S_b^0 - L_b \cdot \kappa, \tag{4}$$

where the subscript b refers to the burned mixture, the superscript 0 indicates a zero-stretch quantity, L_b is the Markstein length, and κ is the stretch rate. In the case of a spherical flame [13, 17, 45, 46], κ is given by

$$\kappa = 2\frac{S_b}{R_f}, \tag{5}$$

where R_f is the flame radius and S_b is given by

$$S_b = \frac{dR_f}{dt}. \tag{6}$$

Substituting Eqs. (5) and (6) into Eq. (4), and integrating with respect to time gives

$$S_b^0 \cdot t = R_f + 2L_b \cdot \ln\left(R_f\right) + C_{st}, \tag{7}$$

where C_{st} is an integration constant. Least-square fitting can be applied to Eq. (7) to obtain S_b^0 and L_b which are linked respectively to the unstretched flame speed S_u^0 and the unburned Marsktein length L_u through the expansion ratio $\sigma = \rho_u/\rho_b$, where ρ_u and ρ_b are the unburned and burned gas densities, respectively. The Markstein number (Ma_u) can be obtained by dividing the Markstein length by the characteristic unstretched flame thickness (δ_f), i.e.

$$Ma_u = \frac{L_u}{\delta_f}, \tag{8}$$

where δ_f is given by [12, 47]

$$\delta_f = \frac{T_{ad} - T_u}{(dT/dx)_{\max}}, \tag{9}$$

where T_{ad} and T_u are the adiabatic flame temperature and the fresh mixture temperature, respectively.

The evolution of the normalized instantaneous spatial velocity as a function of Karlovitz number (Ka=$\kappa\delta_f/S_b^0$) is shown for several mixtures in Figure 1. In this figure, S_b^0=($S_u^0\sigma$), where S_u^0 was obtained using the freely propagating flame code in Cantera. The maximum temperature gradient was used to track the position of the flame front. Since the system is constant pressure, this is equivalent to tracking the maximum density gradient, and is therefore consistent with experimental measurement techniques reliant on Schlieren photography. At ϕ=0.5 the Markstein length is negative whereas for ϕ=1 and ϕ=3, the

Markstein length is positive. The extrapolated unstretched spatial velocities are close to 1 and are thus consistent with the values calculated using the freely propagating flame code. This is consistent with the results of Aung et al. [17] for H_2-air mixtures. While noting that the influence of extrapolation methods on the extracted laminar flame properties have been extensively studied [20, 48–51], it should be emphasized that the range of data employed is of primary importance for extracting consistent flame properties [52] and Natvel et al. [53] showed that consistent flame speed can be obtained when using only the linear part of the V_S=f(κ) curve.

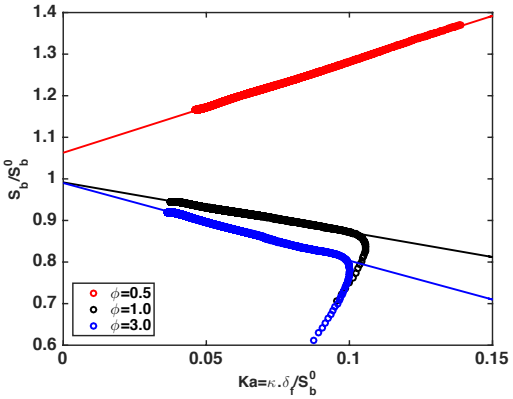

Figure 1: Evolution of the flame speed as a function of Karlovitz number for hydrogen-air spherical flames at T_1=300 K and p_1=101 kPa. Solid lines: linear extrapolation model.

Figure 2 compares some experimental laminar flame speed data [13, 18, 45, 54–57] with the predictions of the numerical simulations. The simulations were performed considering both the mixture-averaged and multi-component transport models. Note that data from Vagelopoulos et al. [55] and Egolfopoulos and Law [56] have been obtained using the counterflow twin-flame technique but were corrected for stretch effects. The predicted flame speed agree qualitatively and quantitatively with the experimental results with a mean absolute error around 5%, regardless of the transport model employed. The largest discrepancy is observed for very lean mixtures with an absolute error of approximately 40-45%. The errors have been calculated by considering an average experimental value for each equivalence ratio. The discrepancies between the predictions and the simulations might be partly attributed to slight differences in the initial temperature employed [58].

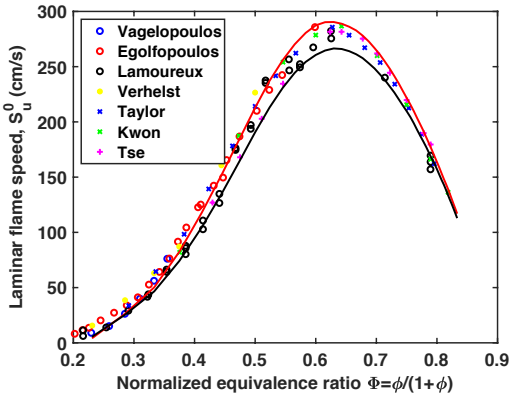

Figure 2: Experimental and calculated laminar flame speed for hydrogen-air mixtures at T_1=300 K and p_1=101 kPa. Solid red line: prediction from USC-Mech II. Red line: mixture-averaged. Black line: multi-component.

Figure 3 compares the calculated and experimental [13, 17, 45, 54, 59] Markstein number for hydrogen-

air flames. For some of the data, it was required to first extract the Markstein length by dividing the provided Markstein numbers by the appropriate flame thickness ($\delta_{fT}=k/(\rho_u c_p)$). This procedure enabled to obtain consistent data but since δ_{fT} depends on the specific thermodynamics and transport data used, it led to the introduction of uncertainty. From the δ_{fT} values provided by Aung et al., this uncertainty was estimated to be of a factor of two or less. The simulations capture the normalized equivalence ratio (Φ) at which the Markstein number changes sign, around Φ=0.4 (ϕ=0.7) as well as the overall evolution of Ma_u with Φ. In particular, it is noted that the "hook" shape of the Markstein number curve on the lean side is well captured. The largest discrepancies are observed on the rich side where the predictions are about three times lower than the measurements. It should be noted however, that the experimental data in this range demonstrate very large scatter. The Markstein numbers predicted for the lean mixtures match relatively well the experimental data. This indicates that the USC-Mech II is well suited to study flame acceleration and DDT processes in highly-unstable lean hydrogen-air mixtures. However, inaccurate prediction of the stability of rich flame might occur. It should also be noted that the predicted Markstein number does not show a strong sensitivity to the transport model employed.

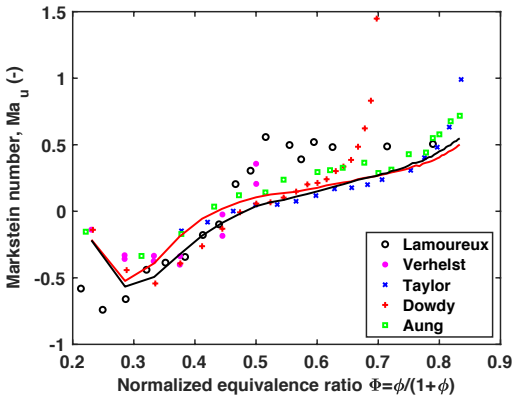

Figure 3: Experimental and calculated Markstein number for hydrogen-air mixtures at T_1=300 K and p_1=101 kPa. Red line: mixture-averaged. Black line: multi-component.

3.2. Lagrangian particles dynamics

To study the thermo-chemical dynamics of Lagrangian particles, two mixtures with ϕ=0.5 (case 1) and ϕ=3 (case 2) have been selected. Their respective predicted Markstein numbers are -0.15 and 0.15. For each mixture, analyses were performed for two particles, one being more stretched (Ma_u=0.075) than the other (Ma_u=0.05). These two flame conditions are referred to as highly and weakly stretched, respectively. The difference of $S_b./S_b^0$ is +5.4% for the lean flame (ϕ=0.5) and -4.6% for the rich flame (ϕ=3.0). Since the two cases are essentially opposite to each other, only the results for the lean mixture are shown in the manuscript. For all figures, the profiles obtained for high and low Ka have been aligned based on their respective time at which the chemical heat release term reaches its maximum.

Figure 4 shows the evolution of the energy terms in Eq. (2) as a function of normalized time for two Lagrangian particles submitted to low and high stretch rate. A diffusion-dominated period (τ_{dif}) has been defined as the difference between the instant at which the diffusion term reaches 10% of its maximum and the time at which it becomes lower than the heat release term. A reaction-dominated period (τ_{reac}) was also defined as the difference between the instant at which the heat release term overcomes the diffusion term and the instant at which it drops below 10% of its maximum. At the beginning of τ_{dif}, the diffusion term is higher for Ka=0.05 whereas at the end of τ_{dif}, it is higher for Ka=0.075. As expected

for flame propagating in a mixture with a negative Markstein length, the heat release rate is higher at high stretch rate during τ_{reac}.

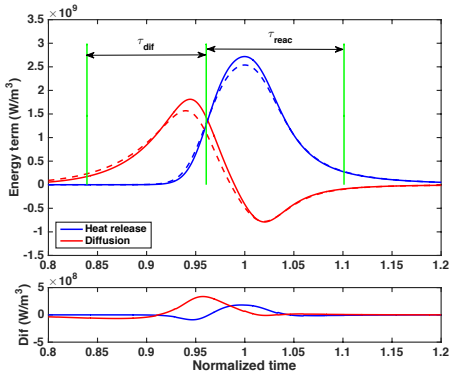

Figure 4: Effect of stretch rate on the magnitude of the energy terms profiles. Two Lagrangian particles entering a hydrogen-air spherical flame are used. Conditions: ϕ=0.5; T_1=300 K and p_1=100 kPa. Ka=0.075: solid lines. Ka=0.05: dashed lines. The green lines indicate the location of the diffusion-dominated and reaction-dominated period obtained for Ka=0.075. The differences (bottom) were obtained by subtracting the value at Ka=0.05 from the value at Ka=0.075.

Details on the heat release dynamics are revealed in Figure 5, which shows the energy release rate per reaction profiles. The dominant reaction is H+O_2(+M)=HO_2(+M) for both Ka. At the beginning of τ_{dif}, the absolute energy release rate per reaction is higher for Ka=0.05 than for Ka=0.075, for all reactions. By the end of τ_{dif}, the absolute energy release per reaction becomes higher for Ka=0.075. During τ_{reac}, OH+H_2=H_2O+H becomes the second highest contributor to the total energy release.

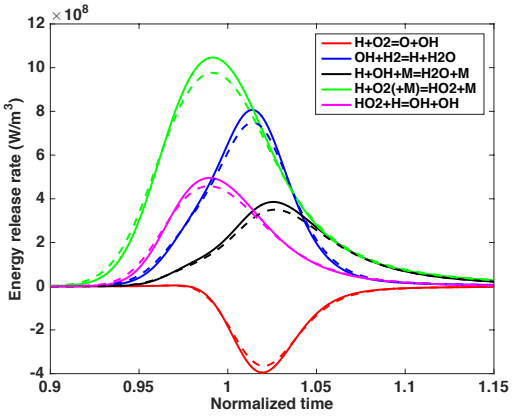

Figure 5: Effect of stretch rate on the energy release rate per reaction profiles. Two Lagrangian particles entering a hydrogen-air spherical flame are used. Conditions: ϕ=0.5; T_1=300 K and p_1=100 kPa. Ka=0.075: solid lines. Ka=0.05: dashed lines.

Figure 6 shows the evolution of the equivalence ratio, temperature and nitrogen mole fraction profiles while Figure 7 shows the species mole fraction profiles. Note that for the temperature profiles, the high stretch rate conditions have been used as the reference. The faster diffusion of hydrogen at low Ka induces a faster drop of the equivalence ratio than at high Ka. This decrease begins long before chemistry is activated and is thus due to the faster mass diffusion of hydrogen molecules. Consistent with the faster diffusion of heat for low Ka in the beginning of τ_{dif}, the temperature increases faster for low Ka and is up to about 30 K higher at the end of τ_{dif}. This results in an earlier activation of the chemistry with production of water vapor and of hydrogen peroxide. Since less fresh mixture has been consumed or diffused away, the reactivity of the mixture entering the reaction-dominated zone is

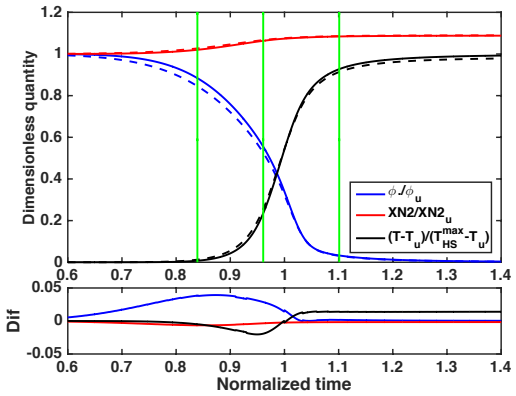

Figure 6: Effect of stretch rate on the equivalence ratio, temperature and nitrogen mole fraction profiles. Two Lagrangian particles entering a hydrogen-air spherical flame are used. Conditions: ϕ=0.5; T_1=300 K and p_1=100 kPa. Ka=0.075: solid lines. Ka=0.05: dashed lines. The green lines indicate the location of the diffusion-dominated and reaction-dominated period obtained for Ka=0.075. HS indicates high stretch. The differences (bottom) were obtained by subtracting the value at Ka=0.05 to the value at Ka=0.075.

higher at high Ka than at low Ka. This leads to a faster temperature increase for high Ka due to the higher chemical energy release rate induced by higher active radical, H and OH, concentrations. The final temperature is approximately 30 K higher for Ka=0.075 than for Ka=0.05.

The chemical dynamics of the active radicals have been further examined by calculating the rate of production (ROP) as shown in Figure 8 for H atoms and Figure 9 for hydroxyl radicals. The H production is dominated by OH+H_2=H+H_2O and O+H_2=H+OH while its consumption is dominated by H+O_2(+M)=HO_2(+M) during τ_{dif} and by H+O_2=O+OH during τ_{reac}. The production of OH is dominated by HO_2+H=OH+OH during τ_{dif} and by the chain branching reactions during τ_{reac}, whereas its consumption is essentially due to OH+H_2=H+H_2O. Except at the beginning of τ_{dif} and at the end of τ_{reac}, the absolute ROP for all the reactions are higher for Ka=0.075. The ROP results demonstrates the importance of low-temperature pathways (H+O_2(+M)=HO_2(+M) followed by HO_2+H=OH+OH) for the chemical dynamics of these lean hydrogen-air flames.

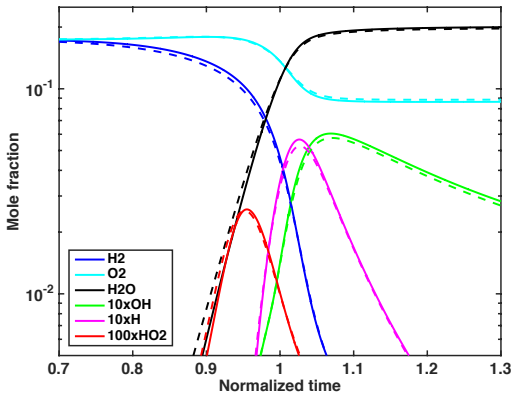

Figure 7: Effect of stretch rate on the species mole fraction profiles. Two Lagrangian particles entering a hydrogen-air spherical flame are used. Conditions: ϕ=0.5; T_1=300 K and p_1=100 kPa. Ka=0.075: solid lines. Ka=0.05: dashed lines.

In their study, Aung et al. [17] explained the higher flame propagation speed for unstable hydrogen-air mixtures by the formation of a "more nearly stoichiometric" mixture due to the preferential diffusion of hydrogen. This implies that a richer mixture than the initial mixture has been formed. However,

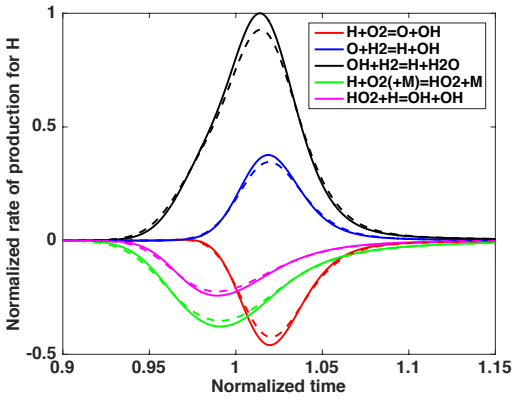

Figure 8: Effect of stretch rate on the H rate of production profiles. Two Lagrangian particles entering a hydrogen-air spherical flame are used. Conditions: ϕ=0.5; T_1=300 K and p_1=100 kPa. Ka=0.075: solid lines. Ka=0.05: dashed lines.

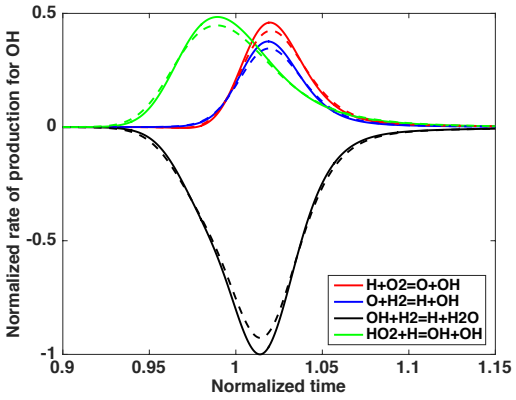

Figure 9: Effect of stretch rate on the OH rate of production profiles. Two Lagrangian particles entering a hydrogen-air spherical flame are used. Conditions: ϕ=0.5; T_1=300 K and p_1=100 kPa. Ka=0.075: solid lines. Ka=0.05: dashed lines.

the present Lagrangian-based approach provides a different perspective. Whatever the stretch rate is, a leaner mixture is formed in the Lagrangian particles as compared to the initial mixture. At high stretch rates, diffusion of hydrogen is slower than at low stretch rates. Consequently, a less lean mixture is formed at high stretch rates compared to low stretch rates. Since this less lean mixture is more reactive, a higher propagation speed is observed. For rich mixtures, the equivalence ratio is also decreasing as compared to the initial one at all stretch rates. However, diffusion is faster at high stretch rates and thus a more lean and more reactive mixture is formed as compared to the initial mixture than at low stretch rates.

4. CONCLUSIONS

In the present study, unsteady Lagrangian-based one-dimensional simulations of spherically expanding flames propagating in hydrogen-air mixtures have been performed. While satisfactory agreement with the available experimental results was observed for the unstretched laminar flame speed, discrepancies were seen for the Marsktein number on the rich side. This is an important aspect since it can lead to inaccurate prediction of the stability of rich flames, which can be detrimental to the prediction of flame acceleration and the DDT process. Detailed analyses of the energy release and chemical dynamics were

performed for two Lagrangian particles subjected to high and low stretch rates. For the lean mixture, although subtle changes in equivalence ratio, $\Delta(\phi/\phi_1)$<0.05, and temperature, $\Delta(T)$<30 K, were observed for the range of Ka studied, a change of more than 5% in S_b was induced. The Lagrangian-based simulations demonstrated that the diffusion of hydrogen is slower at high stretch rates which leads to the formation of a less lean flame with respect to the initial mixture than at low stretch rates. This results in an increasing flame propagation speed with respect to stretch rate. Opposite conclusions can be drawn for the rich mixture case.

REFERENCES

1. H.K. Abdel-Aal, M. Sadik, M. Bassyouni, and M. Shalabi. A new approach to utilize hydrogen as a safe fuel. *International Journal of Hydrogen Energy*, 30(13):1511–1514, 2005.
2. G Ciccarelli and S Dorofeev. Flame acceleration and transition to detonation in ducts. *Prog. Energy Combust. Sci.*, 34(4):499–550, 2008.
3. P. Dagaut and A. Nicolle. Experimental and detailed kinetic modeling study of hydrogen-enriched natural gas blend oxidation over extended temperature and equivalence ratio ranges. *Proceedings of the Combustion Institute*, 30(2):2631–2638, 2005.
4. J. R. Maughan, J. H. Bowen, D. H. Cooke, and J. J. Tuzson. Reducing Gas Turbine Emissions Through Hydrogen-Enhanced, Steam-Injected Combustion. *Journal of Engineering for Gas Turbines and Power*, 118(1):78–85, 1996.
5. C.-J. Tseng. Effects of hydrogen addition on methane combustion in a porous medium burner. *International Journal of Hydrogen Energy*, 27(6):699–707, 2002.
6. S. R. Bell and M. Gupta. Extension of the lean operating limit for natural gas fueling of a spark ignited engine using hydrogen blending. *Combustion Science and Technology*, 123(1-6):23–48, 1997.
7. R.K. Cheng, D. Littlejohn, P.A. Strakey, and T. Sidwell. Laboratory investigations of a low-swirl injector with h2 and ch4 at gas turbine conditions. *Proceedings of the Combustion Institute*, 32(2):3001–3009, 2009.
8. N. Chaumeix, S. Pichon, F. Lafosse, and C.-E. Paillard. Role of chemical kinetics on the detonation properties of hydrogen /natural gas/air mixtures. *International Journal of Hydrogen Energy*, 32(13):2216–2226, 2007.
9. Z. Huang, J. Wang, B. Liu, K. Zeng, J. Yu, and D. Jiang. Combustion characteristics of a direct-injection engine fueled with natural gas–hydrogen blends under different ignition timings. *Fuel*, 86(3):381–387, 2007.
10. Y.K. Wong and G.A. Karim. An analytical examination of the effects of hydrogen addition on cyclic variations in homogeneously charged compression–ignition engines. *International Journal of Hydrogen Energy*, 25(12):1217–1224, 2000.
11. M. Day, J. Bell, P.-T. Bremer, V. Pascucci, V. Beckner, and M. Lijewski. Turbulence effects on cellular burning structures in lean premixed hydrogen flames. *Combustion and Flame*, 156(5):1035–1045, 2009.
12. G. Jomaas, C. K. Law, and J. K. Bechtold. On transition to cellularity in expanding spherical flames. *Journal of Fluid Mechanics*, 583:1–26, 2007.
13. N Lamoureux, N Djebaïli-Chaumeix, and C E Paillard. Laminar flame velocity determination for H2-air-He-CO2 mixtures using the spherical bomb method. *Exp. Therm. Fluid Sci.*, 27:385–393, 2003.
14. C.R.L. Bauwens, J.M. Bergthorson, and S.B. Dorofeev. Experimental investigation of spherical-flame acceleration in lean hydrogen-air mixtures. *International Journal of Hydrogen Energy*, 42(11):7691–7697, 2017.
15. Sheng Yang, Abhishek Saha, Fujia Wu, and Chung K. Law. Morphology and self-acceleration of expanding laminar flames with flame-front cellular instabilities. *Combustion and Flame*, 171:112–118, 2016.
16. A. Clarke. Calculation and consideration of the lewis number for explosion studies. *Process Safety and Environmental Protection*, 80(3):135–140, 2002.
17. K.T. Aung, M.I. Hassan, and G.M. Faeth. Flame stretch interactions of laminar premixed hydrogen/air flames at normal temperature and pressure. *Combustion and Flame*, 109(1):1–24, 1997.
18. O.C Kwon and G.M Faeth. Flame/stretch interactions of premixed hydrogen-fueled flames: measurements and predictions. *Combustion and Flame*, 124(4):590–610, 2001.
19. C.J. Sun, C.J. Sung, L. He, and C.K. Law. Dynamics of weakly stretched flames: quantitative description and extraction of global flame parameters. *Combustion and Flame*, 118(1):108–128, 1999.
20. E. Varea, J. Beeckmann, H. Pitsch, Z. Chen, and B. Renou. Determination of burning velocities from spherically expanding h2/air flames. *Proceedings of the Combustion Institute*, 35(1):711–719, 2015.
21. B Rogg and W Wang. *Run-1DL User Manual*. Lehrstuhl fur Stromungsmechanik Institut fur Thermo-und Fluiddynamik, Ruhr-Universitat Bochum, D-44780 Bochum, Germany, 1995.
22. S Paolucci. On the filtering of sound from the Navier-Stokes equations. Technical report, Livermore, CA, 1982.
23. B. M. Maxwell and M. I. Radulescu. Ignition limits of rapidly expanding diffusion layers: Application to unsteady hydrogen jets. *Combust. Flame*, 158(10):1946–1959, 2011.

24. B. M. Maxwell, R. R. Bhattacharjee, S. S. M. Lau-Chapdelaine, S. A. E. G. Falle, G. J. Sharpe, and M. I. Radulescu. Influence of turbulent fluctuations on detonation propagation. *J. Fluid Mech.*, 818:646–696, 2017.
25. L. P. H. de Goey and L. P. H. de Goey. Mass burning rate of premixed stretched flames: integral analysis versus large-activation-energy asymptotics. *Journal of Engineering Mathematics*, 62:67–84, 2008.
26. J. Yuan, S.D. Tse, and C.K. Law. Dynamics of flame-ball formation from localized ignition: Effects of elevated pressure and temperature. *Proceedings of the Combustion Institute*, 29(2):2501–2507, 2002.
27. O. C. Kwon. Dynamic properties of outwardly propagating spherical hydrogen-air flames at high temperatures and pressures. *KSME International Journal*, 18:325–334, 2004.
28. S.D. Tse and H. Zhao. Dynamics of flame propagation from localized ignition in rich hydrogen/air mixtures: Effects of elevated pressure and temperature. *Combustion Science and Technology*, 177(3):559–578, 2005.
29. V. Ratna Kishore, M. R. Ravi, and A. Ray. Effect of hydrogen content and dilution on laminar burning velocity and stability characteristics of producer gas-air mixtures. *International Journal of Reacting Systems*, 2008:1–8, 2008.
30. C. Prathap, A. Ray, and M.R. Ravi. Investigation of nitrogen dilution effects on the laminar burning velocity and flame stability of syngas fuel at atmospheric condition. *Combustion and Flame*, 155(1):145–160, 2008.
31. C. Prathap, A. Ray, and M.R. Ravi. Effects of dilution with carbon dioxide on the laminar burning velocity and flame stability of h2–co mixtures at atmospheric condition. *Combustion and Flame*, 159(2):482–492, 2012.
32. R J Leveque. *Finite Volume Methods for Hyperbolic Problems*. Cambridge University Press, New York, 2002.
33. J. C. Tannehill, D. A. Anderson, and R. H. Pletcher. *Computational Fluid Mechanics and Heat Transfer,Series in computational and physical processes in mechanics and thermal sciences*. 2nd edition edition, 1997.
34. S D Cohen and A C Hindmarsh. CVODE: A stiff/nonstiff ODE solver in C. *Computers in Physics*, 10 (2):138–143, 1996.
35. L. Dagum and R. Menon. Openmp: an industry standard api for shared-memory programming. *IEEE Computational Science and Engineering*, 5(1):46–55, 1998.
36. David G. Goodwin, Raymond L. Speth, Harry K. Moffat, and Bryan W. Weber. Cantera: An object-oriented software toolkit for chemical kinetics, thermodynamics, and transport processes. https://www.cantera.org, 2018. Version 2.4.0.
37. J. Warnatz. *Inuence of Transport Models and Boundary Conditions on Flame Structure*, pages 87–111. Vieweg+Teubner Verlag, Wiesbaden, 1982.
38. R. J. Kee, J. Warnatz, and J. A. Miller. Fortran computer-code package for the evaluation of gas-phase viscosities, conductivities, and diffusion coefficients. [CHEMKIN]. Technical Report SAND-83-8209, Sandia National Labs., Livermore, CA (USA), 1983.
39. G. Dixon-Lewis. Flame structure and flame reaction kinetics ii: Transport phenomena in multicomponent systems. *Proceedings of the Royal Society of London. Series A. Mathematical and Physical Sciences*, 307(1488):111–135, 1968.
40. R Knikker, A Dauptain, B Cuenot, and T Poinsot. Comparison of computational methodologies for ignition of diffusion layers. *Combust. Sci. Tech.*, 175 (10):1783–1806, 2003.
41. S. G. Davis, A. V. Joshi, H. Wang, and F. Egolfopoulos. An optimized kinetic model of H2/CO combustion. *Proceedings of the Combustion Institute*, 30(1):1283–1292, 2005.
42. G.I. Sivashinsky. On a distorted flame front as a hydrodynamic discontinuity. *Acta Astronautica*, 3(11):889–918, 1976.
43. M. Matalon and B. J. Matkowsky. Flames as gasdynamic discontinuities. *Journal of Fluid Mechanics*, 124:239–259, 1982.
44. Paul Clavin. Dynamic behavior of premixed flame fronts in laminar and turbulent flows. *Progress in Energy and Combustion Science*, 11(1):1–59, 1985.
45. D Dowdy, D Smith, S Taylor, and A Williams. The use of expanding spherical flames to determine burning velocities and stretch effects in hydrogen/air mixture. *Proc. Combust. Inst.*, 23:325–332, 1990.
46. S. Jerzembeck, M. Matalon, and N. Peters. Experimental investigation of very rich laminar spherical flames under microgravity conditions. *Proceedings of the Combustion Institute*, 32(1):1125–1132, 2009.
47. T Poinsot and D Veynante. *Theoretical and Numerical Combustion*. Edwards, 2nd edition, 2005.
48. Z. Chen. On the accuracy of laminar flame speeds measured from outwardly propagating spherical flames: Methane/air at normal temperature and pressure. *Combustion and Flame*, 162(6):2442–2453, 2015.
49. F. Wu, W. Liang, Z. Chen, Y. Ju, and C. K. Law. Uncertainty in stretch extrapolation of laminar flame speed from expanding spherical flames. *Proceedings of the Combustion Institute*, 35(1):663–670, 2015.
50. Z. Chen. On the extraction of laminar flame speed and markstein length from outwardly propagating spherical flames. *Combustion and Flame*, 158(2):291–300, 2011.
51. W. Liang, F. Wu, and C. K. Law. Extrapolation of laminar flame speeds from stretched flames: Role of finite flame thickness. *Proceedings of the Combustion Institute*, 36(1):1137–1143, 2017.
52. A. N. Lipatnikov, S. S. Shy, and W.-Y. Li. Experimental assessment of various methods of determination of laminar flame speed in experiments with expanding spherical flames with positive markstein lengths. *Combustion and Flame*, 162(7):2840–2854, 2015.
53. D. Nativel, M. Pelucchi, A. Frassoldati, A. Comandini, A. Cuoci, E. Ranzi, N. Chaumeix, and T. Faravelli. Laminar flame speeds of pentanol isomers: An experimental and modeling study. *Combustion and Flame*, 166:1–18, 2016.
54. S Verhelst, R Woolley, M Lawes, and R Sierens. Laminar and unstable burning velocities and markstein lengths of hydrogen-air mixtures at engine-like conditions. *Proc. Combust. Inst.*, 30:209–216, 2005.

55. C Vagelopoulos, F Egolfopoulos, and C Law. Further considerations on the determination of laminar flame speeds with the counterflow twin-flame technique. *Proc. Combust. Inst.*, 25:1341–1347, 1994.
56. F Egolfopoulos and C Law. An experimental and computational study of the burning rates of ultra-lean to moderately-rich H2/O2/N2 laminar flames with pressure variations. *Proc. Combust. Inst.*, 23:333–340, 1991.
57. S.D. Tse, D.L. Zhu, and C.K. Law. Morphology and burning rates of expanding spherical flames in h2/o2/inert mixtures up to 60 atmospheres. *Proceedings of the Combustion Institute*, 28(2):1793–1800, 2000.
58. C. Xiouris, T. Ye, J. Jayachandran, and F. N. Egolfopoulos. Laminar flame speeds under engine-relevant conditions: Uncertainty quantification and minimization in spherically expanding flame experiments. *Combustion and Flame*, 163:270–283, 2016.
59. S. C. Taylor. *Burning velocity and the influence of flame stretch*. PhD thesis, 1991.